From carriers and virtual excitons to exciton populations: Insights into time-resolved ARPES spectra from an exactly solvable model

G. Stefanucci and E. Perfetto
Dipartimento di Fisica, Università di Roma Tor Vergata, Via della Ricerca Scientifica 1, 00133 Rome, Italy
and INFN, Sezione di Roma Tor Vergata, Via della Ricerca Scientifica 1, 00133 Rome, Italy

(Received 8 April 2021; revised 17 May 2021; accepted 20 May 2021; published 1 June 2021)

We calculate the *exact* time-resolved ARPES spectrum of a two-band model semiconductor driven out of equilibrium by resonant and nonresonant laser pulses, highlighting the effects of phonon-induced decoherence and relaxation. *Resonant* excitations initially yield a replica of the *valence* band shifted upward by the energy of the exciton peak in photoabsorption. This phase is eventually destroyed by phonon-induced decoherence: The valence-band replica lowers in energy by the Stokes shift, locating at the energy of the exciton peak in photoluminescence, and its width grows due to phonon dressing. *Nonresonant* excitations initially yield a map of the conduction band. Then electrons transfer their excess energy to the lattice and bind with the holes left behind to form excitons. In this relaxed regime a replica of the *conduction* band appears inside the gap. At fixed momentum the lineshape of the conduction-band replica versus the photoelectron energy is proportional to the exciton wave function in "energy space" and it is highly asymmetric. Although the two-band model represents an oversimplified description of real materials, the highlighted features are qualitative in nature; hence they provide useful insights into time-resolved ARPES spectra and their physical interpretation.

DOI: 10.1103/PhysRevB.103.245103

I. INTRODUCTION

Time-resolved and angle-resolved photoemission spectroscopy (trARPES) is currently one of the most flourishing playground for condensed-matter theoreticians. Accurate approximations to the fundamental equations of many-body theory are being incessantly developed to relate the intensity and direction of the photocurrent to the behavior of quantum matter in equilibrium as well as nonequilibrium conditions. The relationship between pseudogap, charge ordering and Fermi arcs in high temperature superconductors [1,2], Auger scattering, electron-phonon coupling, plasmonic excitations, and local screening in core excited metals [3–5], carrier populations and conduction states in excited semiconductors [6–10], topological order [11], excitonic insulator phases [12,13], excitonic Mott transitions [14], and exciton dynamics [15–24] in pumped semiconductors is a nonexhaustive list of the plethora of different phenomena leaving distinctive footprints in trARPES spectra.

The interest in the exciton dynamics of (low-dimensional) semiconductors is steadily gaining momentum, especially due to potentially revolutionary applications in optoelectronics [25]. However, the physical interpretation of trARPES spectra is still subject of debates. The main difficulty in developing accurate many-body schemes suitable for numerical implementations lies in the treatment of electron-electron and electron-phonon scatterings under nonequilibrium conditions. We find useful to distinguish between two different nonequilibrium regimes: the linear-response regime, where the photocurrent is proportional to the intensity of the *pump* field, and the nonlinear regime. Making predictions in the nonlinear regime is certainly more difficult. Calculations are often limited to the quasiequilibrium state of matter, a condition which allows for introducing more or less controlled approximations like, e.g., the invariance under time translations and the fulfillment of the fluctuation-dissipation theorem in different bands. The linear regime offers a wider set of theoretical tools; exciton formation, coherence, and relaxation can be addressed in a more rigorous framework.

The trARPES signatures of excitons in *linearly* excited semiconductors is the topic of this paper. In fact, there still are a few open questions pertaining with two distinct types of excitations. *Resonant* excitations are those of pump pulses with the same frequency as the energy $E^{(\mathrm{x})}$ of a bright exciton. To avoid possible misinterpretations, by $E^{(\mathrm{x})}$ we here denote the energy position of the excitonic peak in the photoabsorption spectrum of the ground-state system. Just after pumping a low-density gas of coherent excitons, also called nonequilibrium excitonic insulator or BEC exciton superfluid, forms [26–31]. Theoretical works [20,22,23,32,33] predict an excitonic sideband in the ARPES spectrum—more precisely a replica of the *valence* band shifted upward by $E^{(\mathrm{x})}$. The subsequent dynamics of the coherent exciton gas involves electron-phonon scatterings [29,34], generation of phonons and phonon-induced decoherence [35], until the formation of a gas of incoherent excitons dressed by phonons, i.e., exciton-polarons. This incoherent phase is expected to set in on a time scale of a few hundreds of femtoseconds [36–39] and it lasts until excitons radiatively recombine [40,41]. To the best of our knowledge no theoretical ARPES studies exist in this phase. Is the excitonic sideband still visible? If so, is it any different

from that of the coherent phase? Does the conduction band appear? Does the phonon bath relax? Besides strengthening our understanding an answer to these questions is becoming urgent. Recent experiments have indeed reported excitonic sidebands in a resonantly pumped WSe_2 monolayer after 0.5 ps [42] and in a WSe_2 bulk until 0.1 ps [43].

The second type of excitation is generated by *nonresonant* pumping. Here the pump frequency is larger than the gap and electrons are promoted to empty conduction states. Just after pumping the ARPES spectrum provides a map of the conduction bands, the signal intensity being proportional to the band-resolved and momentum-resolved carrier populations. The excited electrons soon transfer their energy to the lattice, migrate toward the bottom of the conduction band [7,10], and eventually bind with the left behind hole to form excitons [15,19]. The spectral function in this relaxed (and incoherent) phase has been studied theoretically using the T-matrix approximation in the particle-hole channel assuming a quasithermal equilibrium [20,21,32,44–48]. The theory predicts an excitonic sideband inside the gap, about $E^{(\mathrm{x})}$ above the valence band maximum. However, this spectral structure turns out to be a replica of the *conduction* band [20,21,48]. Could this be the ultimate fate of the excitonic sideband for resonant excitations? May different excitations (resonant versus nonresonant) yield different sidebands (valence replica versus conduction replica) in the relaxed and incoherent phase? Could not the replica of the conduction band be an artifact of the T-matrix approximation in combination with the assumption of quasithermal equilibrium?

We address the above issues through the *exact* analytic solution of a two-band model semiconductor where both electron-electron and electron-phonon interactions are taken into account. As the answer to the asked questions is qualitative in nature, our results provide a useful reference for benchmarking approximate many-body treatments. The main findings of our paper are: (i) Incoherent excitons forming after resonant pumping do only change slightly the replica of the valence band (observed in the coherent phase); in particular the replica lowers in energy by the Stokes shift [49] and its width grows due to phonon dressing (exciton-polarons); (ii) Phonon dressing is much faster than decoherence, the former being dictated by the largest phonon frequency whereas the latter by the smallest polaronic shift; and (iii) Excitons forming after nonresonant pumping give rise to a replica of the conduction band, thus confirming the results of previous studies [20,21,48]; for any fixed momentum the lineshape of the replica is determined by the exciton wave function in "energy space" and it is highly asymmetric.

The organization of the paper is as follows. In Sec. II we introduce the model and set up the problem; we also discuss the behavior of relevant observable quantities in different scenarios. The solution of the model for both acoustic and optical phonons is derived in Sec. III. We defer the reader to the Appendices for the calculation of the spectral function, momentum-resolved electron occupations, polarization, and phonon occupations using the exact many-body wave function. Results for resonant and nonresonant excitations are presented in Secs. IV and V, respectively. A summary of the main findings is drawn in Sec. VI.

II. EXCITON-POLARON MODEL

In standard notation the two-band model Hamiltonian reads

$$\begin{aligned}\hat{H} = &\sum_k \left(\epsilon^c_k \hat{c}^\dagger_k \hat{c}_k + \epsilon^v_k \hat{v}^\dagger_k \hat{v}_k\right) + \sum_q \omega_q \hat{b}^\dagger_q \hat{b}_q \\ &- \frac{1}{\mathcal{N}} \sum_{pk_1k_2} U_p \hat{c}^\dagger_{k_1+p} \hat{v}_{k_2+p} \hat{v}^\dagger_{k_2} \hat{c}_{k_1} \\ &+ \frac{1}{\sqrt{\mathcal{N}}} \sum_{kq} \lambda^k_q (\hat{c}^\dagger_{k+q} \hat{c}_k \hat{b}_q + \hat{c}^\dagger_k \hat{c}_{k+q} \hat{b}^\dagger_q). \end{aligned} \tag{1}$$

The first two terms describe free electrons in the valence (v) or conduction (c) band and free phonons. The remaining terms account for the electron-hole (eh) Coulomb interaction and the electron-phonon interaction; $\mathcal{N}$ is the number of discretized momenta in the first Brillouin zone. In our model only conduction electrons interact with phonons. However, the idea presented below can easily be adapted to include an interaction with valence electrons. The Hamiltonian in Eq. (1) has been studied numerically with quantum Monte Carlo methods to address the dependence of the exciton-polaron wave function on the electron-phonon coupling [50,51]. We are not aware of other exact numerical or analytical treatments.

The state $|\Phi_0\rangle$ with a filled valence band, an empty conduction band and no phonons is an eigenstate of $\hat{H}$. We assume that the interaction U_p is much larger than the energy gap E_g between the conduction and valence bands. Then $|\Phi_0\rangle$ is the ground state and, without any loss of generality, we set to zero its energy. We now consider an ultrafast and low-intensity laser pulse pumping electrons from the valence band to the conduction band. To lowest order in the light intensity the state of the system at the end of the pulse can be written as

$$|\Psi\rangle = \alpha|\Phi_0\rangle + \beta|\Phi_{\mathrm{x}}\rangle, \tag{2}$$

with $\beta = \sqrt{1-\alpha^2} \ll 1$ and

$$|\Phi_{\mathrm{x}}\rangle = \sum_k Y^0_k \hat{c}^\dagger_k \hat{v}_k |\Phi_0\rangle, \tag{3}$$

the component of the full many-body state with one electron in the conduction band, one hole in the valence band, and no phonons. The coefficients Y^0_k depend on the laser pulse parameters, e.g., duration and frequency. The state in Eq. (2) is not, in general, an eigenstate of $\hat{H}$. The pumped electron feels the attractive interaction with the hole left behind and it is scattered by phonons. We shall investigate two different physical scenario.

In the so called resonant case electrons are pumped at the exciton frequency and the state $|\Phi_{\mathrm{x}}\rangle$ is a bright excitonic eigenstate of the electronic part of $\hat{H}$. Discarding the electron-phonon interaction and denoting by $E^{(\mathrm{x})} < E_g$ the exciton energy the evolution of the state $|\Psi\rangle$ would simply be

$$|\Psi(t)\rangle = \alpha|\Phi_0\rangle + \beta e^{-iE^{(\mathrm{x})}t}|\Phi_{\mathrm{x}}\rangle. \tag{4}$$

As $|\Psi(t)\rangle$ has no phonons the electronic-density matrix is a *pure state*

$$\hat{\rho}_{\mathrm{el}}(t) \equiv \mathrm{Tr}_{\mathrm{ph}}\{\,|\Psi(t)\rangle\langle\Psi(t)|\,\} = |\Psi(t)\rangle\langle\Psi(t)|, \tag{5}$$

where $\mathrm{Tr}_{\mathrm{ph}}$ signifies a trace over the phononic degrees of freedom. A system described by Eq. (5) is said to contain *virtual* or *coherent* excitons [52,53]. In fact, it is characterized by coherent oscillations of the polarization since the quantity

$$\mathrm{Tr}_{\mathrm{el}}[\hat{\rho}_{\mathrm{el}}(t)\hat{v}_k^\dagger \hat{c}_k] = \alpha^* \beta\, Y_k^0 e^{-iE^{(\mathrm{x})}t} \tag{6}$$

oscillates at the exciton frequency for all k's, see also Eq. (16) below. In Ref. [33] we argued that these coherent oscillations could be observed in trARPES using ultrafast probes of duration shorter than $2\pi/E^{(\mathrm{x})}$.

The state in Eq. (4) approximates the true time-dependent state only in the early stage of the evolution. Just after pumping electrons and phonons begin to scatter, mutually dressing each others, and the initial coherence is eventually destroyed. The electronic system is expected to evolve toward an *admixture* of $|\Phi_0\rangle$ and some exciton-like states $|\Phi_{\mathrm{x}}^{(i)}\rangle$:

$$\begin{aligned}\hat{\rho}_{\mathrm{el}}(t\to\infty) &= \lim_{t\to\infty} \mathrm{Tr}_{\mathrm{ph}}\{|\Psi(t)\rangle\langle\Psi(t)|\} \\ &= |\alpha|^2\,|\Phi_0\rangle\langle\Phi_0| + |\beta|^2 \sum_i w_i |\Phi_{\mathrm{x}}^{(i)}\rangle\langle\Phi_{\mathrm{x}}^{(i)}|. \end{aligned} \tag{7}$$

In this steady-state regime excitons are said *real* or *incoherent* and one can introduce the concept of *exciton populations* since the polarization does no longer oscillate. However, the existence and the characterization of the steady-state regime has so far been based on reasonable assumptions and it is still subject of debate. The purpose of this paper is to provide useful insights into this issue through the solution of the time-dependent Schrödinger equation.

In the second scenario the laser pulse generates free carriers in the conduction band (nonresonant pumping). It is then expected that carriers give their excess energy to the lattice, thereby migrating toward the bottom of the conduction band and eventually binding with the holes left behind to form excitons. The phonon-driven formation of excitons is another debated topic in the literature as no real-time calculations are available to confirm this picture. Due to the simplicity of the model we could only address the dynamics of free carriers initially at the bottom of the conduction band.

Independently of the scenario we need to calculate the time-evolved state

$$|\Psi(t)\rangle \equiv e^{-i\hat{H}t}|\Psi\rangle = \alpha|\Phi_0\rangle + \beta|\Phi_{\mathrm{x}}(t)\rangle, \tag{8}$$

with

$$|\Phi_{\mathrm{x}}(t)\rangle = e^{-i\hat{H}t}\sum_k Y_k^0 \hat{c}_k^\dagger \hat{v}_k|\Phi_0\rangle. \tag{9}$$

Henceforth we refer to $|\Phi_{\mathrm{x}}(t)\rangle$ as the exciton-polaron state although it may also describe unbound *eh* pairs dressed by phonons. From $|\Phi_{\mathrm{x}}(t)\rangle$ we can monitor the momentum-resolved phonon occupations

$$n_q(t) = \langle\Phi_{\mathrm{x}}(t)|\hat{b}_q^\dagger \hat{b}_q|\Phi_{\mathrm{x}}(t)\rangle, \tag{10}$$

as well as the standard deviation of the phonon momentum

$$\sigma_Q^2(t) = \langle\Phi_{\mathrm{x}}(t)|\hat{Q}^2|\Phi_{\mathrm{x}}(t)\rangle - Q^2(t), \tag{11}$$

where $\hat{Q} = \sum_q q\,\hat{n}_q$ and $Q(t) = \sum_q q\,n_q(t)$. We can also calculate the Green's functions

$$\begin{aligned} G_k^{cc}(t,t') &= i\langle\Psi(t')|\hat{c}_k^\dagger e^{-i\hat{H}(t'-t)}\hat{c}_k|\Psi(t)\rangle \\ &= i|\beta|^2\langle\Phi_{\mathrm{x}}(t')|\hat{c}_k^\dagger e^{-i\hat{H}(t'-t)}\hat{c}_k|\Phi_{\mathrm{x}}(t)\rangle \end{aligned} \tag{12}$$

and

$$\begin{aligned} G_k^{cv}(t,t') &= i\langle\Psi(t')|\hat{v}_k^\dagger e^{-i\hat{H}(t'-t)}\hat{c}_k|\Psi(t)\rangle, \\ &= i\alpha^*\beta\,\langle\Phi_0|\hat{v}_k^\dagger e^{-i\hat{H}(t'-t)}\hat{c}_k|\Phi_{\mathrm{x}}(t)\rangle. \end{aligned} \tag{13}$$

The Green's functions in Eqs. (12) and (13) contain information on the electronic transient spectrum, occupations, and polarization. In fact, the ARPES signal of the system at time T is proportional to the transient spectral function $A_k(T,\omega)$ which is in turn related to the Green's function in Eq. (12) through (for ω above the valence band maximum)

$$A_k(T,\omega) = -i\int d\tau e^{i\omega\tau} G_k^{cc}\Big(T+\frac{\tau}{2}, T-\frac{\tau}{2}\Big). \tag{14}$$

The electron occupations in the conduction band can be obtained from the same Green's function since

$$n_k^c(t) = \langle\Psi(t)|\hat{c}_k^\dagger\hat{c}_k|\Psi(t)\rangle = -iG_k^{cc}(t,t). \tag{15}$$

Denoting by d_k the dipole matrix element between a conduction state and a valence state of momentum k the polarization at time t reads

$$\begin{aligned} P(t) &= \frac{1}{\mathcal{N}}\sum_k d_k\langle\Psi(t)|\hat{v}_k^\dagger\hat{c}_k|\Psi(t)\rangle + \mathrm{H.c.} \\ &= -\frac{i}{\mathcal{N}}\sum_k d_k G_k^{cv}(t,t) + \mathrm{H.c.} \end{aligned} \tag{16}$$

In the next section we expand the exciton-polaron state on a convenient basis and calculate the time-dependent expansion coefficients.

III. TIME-DEPENDENT EXCITON-POLARON WAVE FUNCTION

We introduce the states

$$|kq_1\ldots q_M\rangle = \hat{c}_{k-q_1\ldots-q_M}^\dagger \hat{v}_k \hat{b}_{q_1}^\dagger \ldots \hat{b}_{q_M}^\dagger|\Phi_0\rangle, \tag{17}$$

describing one *eh* pair and M phonons. In terms of these states Eq. (3) can be written as $|\Phi_{\mathrm{x}}\rangle = \sum_k Y_k^0|k\rangle$. Hence the calculation of $|\Phi_{\mathrm{x}}(t)\rangle$ passes through the calculation of $e^{-i\hat{H}t}|k\rangle$. The Hamiltonian $\hat{H}$ maps the space spanned by the states of Eq. (17) onto the same space since

$$\begin{aligned} \hat{H}|kq_1\ldots q_M\rangle &= \Big(\epsilon_{k-q_1\ldots-q_M}^c - \epsilon_k^v + \sum_{j=1}^M \omega_{q_j}\Big)|kq_1\ldots q_M\rangle \\ &\quad - \frac{1}{\mathcal{N}}\sum_p U_p|k+pq_1\ldots q_M\rangle \\ &\quad + \frac{1}{\sqrt{\mathcal{N}}}\sum_{j=1}^M \lambda_{q_j}^k|kq_1\ldots \overset{\sqcap}{q}_j\ldots q_M\rangle \\ &\quad + \frac{1}{\sqrt{\mathcal{N}}}\sum_q \lambda_q^k|kqq_1\ldots q_M\rangle, \end{aligned} \tag{18}$$

where the square-cap symbol "⊓" signifies that the index below it is missing. We can therefore expand the exciton-polaron state as

$$|\Phi_{\rm x}(t)\rangle = \sum_{M=0}^{\infty} \frac{1}{M!} \sum_{k,q_1\ldots q_M} Y_{kq_1\ldots q_M}(t)|kq_1\ldots q_M\rangle. \tag{19}$$

Without any loss of generality we take the amplitudes $Y_{kq_1\ldots q_M}$ totally symmetric under a permutation of the phonon indices $\{q_1,\ldots,q_M\}$; only this irreducible representation contributes in the sum of Eq. (19). Using the inner product,

$$\langle k'q'_1\ldots q'_M|kq_1\ldots q_M\rangle = \delta_{k'k}\sum_P \prod_{j=1}^{M} \delta_{q'_j q_{P(j)}}, \tag{20}$$

where the sum runs over all permutations of $\{1,\ldots,M\}$, we find

$$\langle kq_1\ldots q_M|e^{-i\hat{H}t}|\Phi_{\rm x}\rangle = Y_{kq_1\ldots q_M}(t). \tag{21}$$

Equations (18) and (21) allows for generating a hierarchy of differential equations for the amplitudes

$$\begin{aligned} i\dot{Y}_{kq_1\ldots q_M}(t) &= \langle kq_1\ldots q_M|\hat{H}e^{-i\hat{H}t}|\Phi_{\rm x}\rangle \\ &= \left(\epsilon^c_{k-q_1\ldots-q_M} - \epsilon^v_k + \sum_{j=1}^{M}\omega_{q_j}\right) Y_{kq_1\ldots q_M}(t) \\ &\quad - \frac{1}{\mathcal{N}}\sum_p U_p Y_{k+pq_1\ldots q_M}(t) \\ &\quad + \frac{1}{\sqrt{\mathcal{N}}}\sum_{j=1}^{M}\lambda^k_{q_j} Y_{kq_1\ldots \sqcap \ldots q_M}(t) \\ &\quad + \frac{1}{\sqrt{\mathcal{N}}}\sum_q \lambda^k_q Y_{kqq_1\ldots q_M}(t). \end{aligned} \tag{22}$$

Already at this stage we can discuss the conditions for the development of an incoherent regime. Taking into account Eqs. (8) and (19) we find for the electronic-density matrix

$$\begin{aligned} \hat{\rho}_{\rm el}(t) &= |\alpha|^2|\Phi_0\rangle\langle\Phi_0| \\ &\quad + |\beta|^2\sum_{M=0}^{\infty}\frac{1}{M!}\sum_{q_1\ldots q_M}|\Phi_{{\rm x},q_1\ldots q_M}(t)\rangle\langle\Phi_{{\rm x},q_1\ldots q_M}(t)| \\ &\quad + \left(\beta\alpha^*\sum_k Y_k(t)|k\rangle\langle\Phi_0| + {\rm H.c.}\right), \end{aligned} \tag{23}$$

where we have defined

$$|\Phi_{{\rm x},q_1\ldots q_M}(t)\rangle \equiv \sum_k Y_{kq_1\ldots q_M}(t)|k\rangle. \tag{24}$$

A direct comparison with Eq. (7) shows that for the system to relax toward an incoherent steady-state the zero-phonon amplitude $Y_k(t)$ must vanish as $t\to\infty$ and

$$\lim_{t\to\infty}\sum_{M=0}^{\infty}\frac{1}{M!}\sum_{q_1\ldots q_M} Y_{kq_1\ldots q_M}(t)Y^*_{k'q_1\ldots q_M}(t) = \sum_i w_i \mathcal{Y}^i_k \mathcal{Y}^{i*}_{k'}, \tag{25}$$

where $\mathcal{Y}^i_k$ are some k-dependent and time-independent complex quantities. We shall comment on the fulfillment of these properties using the exact solution.

The hierarchy in Eq. (22) can be solved analytically in some special, yet relevant, cases. The first condition to meet is

$$\epsilon^c_{k-q_1\ldots-q_M} = \epsilon^c_k, \tag{26}$$

for all $\{q_1,\ldots,q_M\}$ and for all M. Rigorously this condition is satisfied only for a perfectly flat conduction band. However, Eq. (26) is a good approximation for couplings λ's and frequencies ω's such that the distribution of phonon-momenta has a peak around $q=0$ with standard deviation σ_Q much smaller than the momentum-scale over which the dispersion ϵ^c_k varies. No restrictions on the dispersion of the valence band ϵ^v_k are imposed.

Let us introduce the vectors

$$(\mathbf{Y}_{q_1\ldots q_M})_k = Y_{kq_1\ldots q_M} \tag{27}$$

and the matrices

$$\mathbb{H}_{kk'} = \delta_{kk'}\left(\epsilon^c_k - \epsilon^v_k\right) - \frac{U_{p-k}}{\mathcal{N}} \quad ; \quad \mathbb{L}_{q,kk'} = \delta_{kk'}\lambda^k_q. \tag{28}$$

Then the hierarchy in Eq. (22) can be rewritten in matrix form as (omitting the dependence on time)

$$\begin{aligned} i\dot{\mathbf{Y}}_{q_1\ldots q_M} &= (\mathbb{H} + \omega_{q_1}\ldots+\omega_{q_M})\mathbf{Y}_{q_1\ldots q_M} \\ &\quad + \sum_{j=1}^{M}\frac{\mathbb{L}_{q_j}}{\sqrt{\mathcal{N}}}\mathbf{Y}_{q_1\ldots\sqcap\ldots q_M} + \sum_q\frac{\mathbb{L}_q}{\sqrt{\mathcal{N}}}\mathbf{Y}_{qq_1\ldots q_M}. \end{aligned} \tag{29}$$

Notice that the matrix $\mathbb{H}$ is the Bethe-Salpeter Hamiltonian for an *eh* pair. Hence the spectrum of $\mathbb{H}$ consists of a discrete excitonic part with subgap eigenvalues and a continuum *eh* part with eigenvalues larger than the gap.

A. q-independent coupling

We consider optical phonons $\omega_q = \omega_0$ and coupling matrices $\mathbb{L}_q = \mathbb{L}$ depending only on the electron momentum, hence $\lambda^k_q = \lambda^k$. In this case all coefficients of the hierarchy are independent of the phonon momenta. We look for solutions of the form

$$\mathbf{Y}_{q_1\ldots q_M}(t) = \sqrt{\frac{M!}{\mathcal{N}^M}}\mathbf{Y}_M(t). \tag{30}$$

Inserting Eq. (30) into Eq. (29) we find a closed system of equations for the $\mathbf{Y}_M$'s

$$i\dot{\mathbf{Y}}_M = (\mathbb{H} + M\omega_0)\mathbf{Y}_M + \sqrt{M}\mathbb{L}\mathbf{Y}_{M-1} + \sqrt{M+1}\mathbb{L}\mathbf{Y}_{M+1}. \tag{31}$$

This simplified hierarchy can easily be solved with continued matrix fraction techniques [54,55]. The time evolved state in Eq. (19) then reads

$$|\Phi_{\rm x}(t)\rangle = \sum_{M=0}^{\infty}\sum_k \frac{Y_{kM}(t)}{\sqrt{M!}}|kM\rangle, \tag{32}$$

where

$$|kM\rangle \equiv \frac{1}{\sqrt{\mathcal{N}^M}}\sum_{q_1\ldots q_M}|kq_1\ldots q_M\rangle. \tag{33}$$

For arbitrary initial conditions $\mathbf{Y}_M(0) = \delta_{M0}\mathbf{Y}^0$ no steady state is ever attained in the long time limit. This means that the electronic-density matrix does not evolve toward an admixture

like in Eq. (7). Nonetheless, the spectral function $A_k(T,\omega)$ becomes independent of T as $T\to\infty$ if the probing time, i.e., the τ window of integration in Eq. (14), is much longer than $2\pi/\omega_0$.

It is instructive to expand the vectors $\mathbf{Y}_M$ in eigenvectors $\mathbf{Y}^{(\mu)}$ with energies $E^{(\mu)}$ of the Bethe-Salpeter Hamiltonian $\mathbb{H}$

$$\mathbf{Y}_M(t)=\sum_\mu \alpha_{\mu M}(t)\mathbf{Y}^{(\mu)}. \tag{34}$$

The hierarchy in Eq. (31) can be used to obtain a hierarchy for the coefficients of the expansion

$$i\dot\alpha_{\mu M}=(E^{(\mu)}+M\omega_0)\alpha_{\mu M} + \sum_\nu L_{\mu\nu}[\sqrt{M}\alpha_{\nu M-1}+\sqrt{M+1}\alpha_{\nu M+1}], \tag{35}$$

where we have defined

$$L_{\mu\nu}\equiv \mathbf{Y}^{(\mu)\dagger}\mathbb{L}\mathbf{Y}^{(\nu)}. \tag{36}$$

If the coupling λ^k depends on k then the matrix element $L_{\mu\nu}$ is, in general, nonvanishing for $\mu\neq\nu$. This implies that even if the initial condition $\mathbf{Y}_0(0)=\mathbf{Y}^{(\mu_0)}$ is an eigenstate of $\mathbb{H}$, hence $\alpha_{\mu M}(0)=\delta_{0M}\delta_{\mu_0\mu}$, electronic states with $\nu\neq\mu_0$ are visited during the evolution.

B. *k*-independent coupling

The hierarchy in Eq. (29) can be solved also in the special case $\mathbb{L}_q=\lambda_q\mathbb{1}$, i.e., for an electron-phonon coupling $\lambda_q^k=\lambda_q$ independent of the electronic momentum. No restrictions on the phonon frequencies is necessary in this case. We define

$$\mathbf{Y}_{q_1\ldots q_M}(t)=e^{-i\mathbb{H}t}\,\mathbf{X}_{q_1\ldots q_M}(t), \tag{37}$$

and rewrite the hierarchy for the vectors $\mathbf{X}$'s

$$i\dot{\mathbf{X}}_{q_1\ldots q_M}=(\omega_{q_1}\ldots+\omega_{q_M})\mathbf{X}_{q_1\ldots q_M} + \sum_{j=1}^{M}\frac{\lambda_{q_j}}{\sqrt{\mathcal{N}}}\mathbf{X}_{q_1\ldots\sqcap_j\ldots q_M}+\sum_q\frac{\lambda_q}{\sqrt{\mathcal{N}}}\mathbf{X}_{qq_1\ldots q_M}. \tag{38}$$

We look for solutions of the form

$$\mathbf{X}_{q_1\ldots q_M}(t)=f_{q_1}(t)\ldots f_{q_M}(t)\mathbf{X}(t). \tag{39}$$

Inserting Eq. (39) into Eq. (38) we find that the hierarchy is solved provided that

$$i\dot f_q=\frac{\lambda_q}{\sqrt{\mathcal{N}}}+\omega_q f_q, \tag{40}$$

and

$$i\dot{\mathbf{X}}=\sum_q\frac{\lambda_q}{\sqrt{\mathcal{N}}}f_q(t)\mathbf{X}. \tag{41}$$

The solution of Eq. (40) with boundary condition $f_q(0)=0$ (no phonons at the initial time) is the Langreth function [56]

$$f_q(t)=\frac{1}{\sqrt{\mathcal{N}}}\frac{\lambda_q}{\omega_q}(e^{-i\omega_q t}-1). \tag{42}$$

Substituting the explicit form of $f_q(t)$ into Eq. (41) we find

$$\mathbf{X}(t)=\ell(t)\mathbf{X}(0), \tag{43}$$

with

$$\ell(t)=\exp\left[\frac{1}{\mathcal{N}}\sum_q\left(\frac{\lambda_q}{\omega_q}\right)^2(-1+e^{-i\omega_q t}+i\omega_q t)\right]. \tag{44}$$

Taking into account Eqs. (37) and (39) we eventually get

$$\mathbf{Y}_{q_1\ldots q_M}(t)=f_{q_1}(t)\ldots f_{q_M}(t)\ell(t)\mathbf{Y}^0(t), \tag{45}$$

where $\mathbf{Y}^0(t)=e^{-i\mathbb{H}t}\mathbf{Y}^0$ and $(\mathbf{Y}^0)_k=Y_k^0$ are the amplitudes of the state $|\Phi_{\rm x}\rangle$. In Eq. (45) the phonon dynamics is decoupled from the electron dynamics. If the initial state is an eigenstate of $\mathbb{H}$, i.e., $\mathbf{Y}^0=\mathbf{Y}^{(\mu_0)}$ then no other electronic state is visited at later times.

For acoustic phonons the function $\ell(t)$ vanishes as $t\to\infty$ and therefore $Y_k(t)=\ell(t)Y_k^0(t)$ vanishes too in the same limit. This implies that the electronic-density matrix becomes an admixture in the long-time limit, see Eq. (23). To determine the nature of this admixture we have to evaluate Eq. (25). Taking into account that $|\ell(t)|^2=\exp[-\sum_q|f_q(t)|^2]$, it is straightforward to find

$$\lim_{t\to\infty}\hat\rho_{\rm el}(t)=|\alpha|^2|\Phi_0\rangle\langle\Phi_0|+|\beta|^2|\Phi_{\rm x}^{(0)}(t)\rangle\langle\Phi_{\rm x}^{(0)}(t)| \tag{46}$$

with $|\Phi_{\rm x}^{(0)}(t)\rangle=\sum_k Y_k^0(t)|k\rangle$. Therefore the admixture contains only two states and for it to attain a steady state the initially pumped state must be an eigenstate of the electron Hamiltonian $\mathbb{H}$. In particular if the initial state is the excitonic eigenstate then $Y_k^0(t)=e^{-iE^{(\rm x)}t}Y_k^{(\rm x)}$ and

$$\lim_{t\to\infty}\hat\rho_{\rm el}(t)=|\alpha|^2|\Phi_0\rangle\langle\Phi_0|+|\beta|^2|\Phi_{\rm x}\rangle\langle\Phi_{\rm x}|. \tag{47}$$

Comparing this result with the electronic-density matrix at the initial time, see Eqs. (4) and (5), we conclude that the two-band model is able to describe the complete loss of coherence due to scattering of electrons with acoustic phonons.

IV. RESONANT PUMPING

We investigate the effects of phonon dressing and decoherence in a semiconductor driven by coherent light of frequency in resonance with the energy of a bright exciton (resonant pumping). For illustration we consider a 1D model with a flat conduction band $\epsilon_k^c=\epsilon_c=E_g/2$ [conduction band minimum (CBM) at $E_g/2$] and a dispersive valence band $\epsilon_k^v=E_g[\cos k-1]-E_g/2$ [valence band maximum (VBM) at $-E_g/2$] separated by an energy gap E_g. Henceforth all energies are measured in units of E_g and times in units of $1/E_g$. For a short-range (momentum-independent) Coulomb interaction $U_p=U=0.65$ the electronic system admits an exciton state $\mathbf{Y}^{(\rm x)}$ of energy $E^{(\rm x)}\simeq 0.81$. Under the condition of resonant pumping the initial state is therefore $\mathbf{Y}^0=\mathbf{Y}^{(\rm x)}$.

Without electron-phonon scattering, i.e., $\lambda_q^k=0$, the spectral function $A_k(T,\omega)$ in Eq. (14) is independent of T and for each k it exhibits a single peak at energy $\epsilon_k^v+E^{(\rm x)}$ [20,22,23,32], see also Appendix A:

$$A_k(T,\omega)=2\pi|\beta|^2\left|Y_k^{(\rm x)}\right|^2\delta\left(\omega-\epsilon_k^v-E^{(\rm x)}\right). \tag{48}$$

This spectral function can be interpreted as the fully interacting spectral function just after the excitation, i.e., at $T=0$; phonon scatterings kick in only at later times. Equation (48) yields an excitonic sideband; it is a replica of the valence band

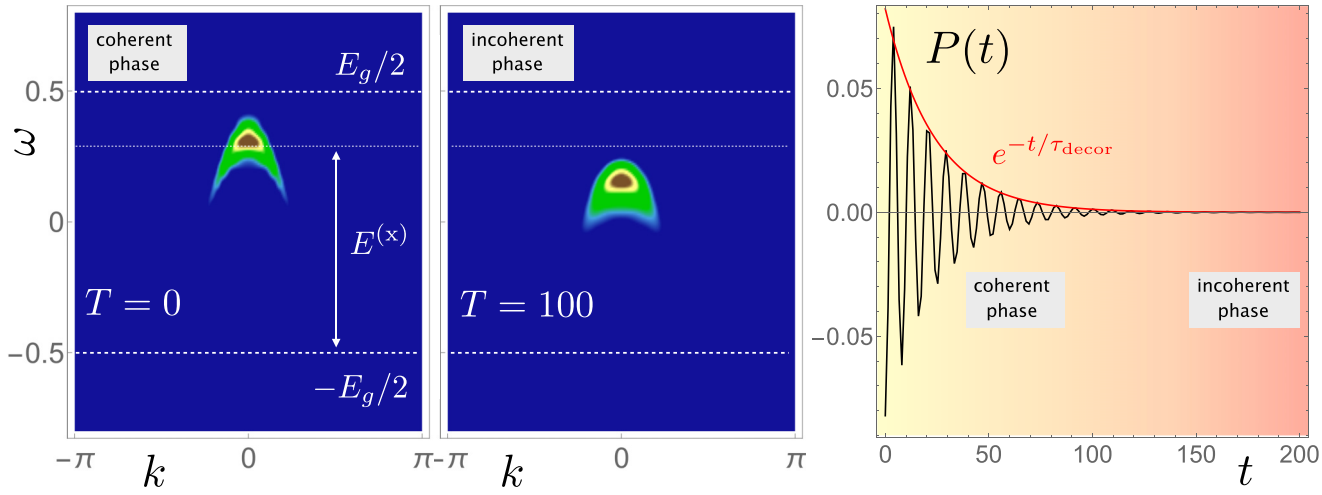

FIG. 1. Spectral function of the interacting electron-phonon system for $T = 0$ (left) and $T = 100$ (middle). Tick-dashed lines have been drawn in correspondence of the CBM and VBM. Thin-dashed lines have been drawn in correspondence of the exciton energy. The right panel shows the time-dependent polarization calculated with $d_k = d$ for all k points.

located at energy $E^{(x)}$ above the VBM with spectral weight proportional to the square of the excitonic wave function. In Fig. 1 (left) we show the color plot of Eq. (14). Calculations have been performed with $\mathcal{N} = 81$ k-points using a τ window of integration that extends from $\tau_{\min} = -60$ to $\tau_{\max} = -\tau_{\min}$.

The electron-phonon coupling causes the spectral function to acquire a dependence on T, even for initial states that are eigenstates of $\mathbb{H}$. We study the evolution of the system when conduction electrons interact through a coupling $\lambda_q = \frac{\lambda_0}{2}(\cos q + 1)$ with acoustic phonons of dispersion $\omega_q = \omega_s \sin|q|$. In the numerical simulations we have chosen $\lambda_0 = 0.18$ and $\omega_s = 2(E_g - E^{(x)}) = 0.38$, which is twice the exciton binding energy. In Appendix B we demonstrate that the polarization $P(t)$ in Eq. (16) can be written as

$$P(t) = \alpha^* \beta \frac{1}{\mathcal{N}} \sum_k d_k Y_k(t) + \text{H.c.}, \tag{49}$$

where $Y_k(t) = \ell(t) e^{-iE^{(x)}t} Y_k^0$, see Eq. (45). Let us briefly discuss the behavior of $P(t)$ for a vanishing electron-phonon coupling. In this case $\ell(t) = 1$ and the polarization oscillates monochromatically at frequency $E^{(x)}$. In the diagrammatic nonequilibrium Green's function theory a simple Hartree-Fock (HF) treatment of the Coulomb interaction is enough to reproduce the oscillatory behavior [23,26,57–59]. Interestingly, the HF theory also predicts the appearance of the excitonic sideband in the spectral function, see Eq. (48). The coherent oscillations of $P(t)$ are crucial to observe this effect, which does indeed originate from the eigenvalues of the HF Floquet Hamiltonian [60]. Switching on the electron-phonon coupling the function $\ell(t)$, and hence the amplitude $Y_k(t)$, vanishes for $t \to \infty$. In Fig. 1 (right) we show $P(t)$ for a system with dipole matrix elements $d_k = d$ for all k. For $t \simeq 100$ the polarization is suppressed by about two order of magnitudes. We shall show that in this incoherent phase (times $t > 100$) the spectral function still exhibits an excitonic sideband. Therefore excitonic structures in the spectral function are not a hallmark of excitonic coherence, as it is erroneously predicted by the HF theory.

To obtain the spectral function in the incoherent regime we evaluated Eq. (14), see Appendix A, at $T = 100$ using the same τ window of integration as in the left panel of Fig. 1. The result is shown in the middle panel of the same figure. The excitonic sideband is still clearly visible although it is slightly shifted downward. In fact, it would be more appropriate to refer to this spectral feature as the *exciton-polaron sideband*. The experiment of Ref. [42] has most likely measured such sideband as the system was probed after 0.5 ps from the resonant excitation. We also observe that phonon-dressing is responsible for an energy broadening of the sideband, consistently with the reported damping of the polarization.

The energy shift of the excitonic sideband as the system evolves from the coherent to the incoherent phase can be related to the Stokes shift [49]. At zero momentum the coherent peak is detected at energy $E^{(x)}$, i.e., at the onset of the photoabsorption spectrum, whereas the incoherent peak is red shifted by the "reorganization energy", i.e., the energy gain in the transition from an exciton to an exciton-polaron. Therefore the energy of the incoherent peak lies at the onset of the photoluminescence spectrum [61,62]. This also agrees with the fact that the photoluminescence signal is proportional to the population of (incoherent) excitons [34]. In this respect trARPES provides a unique investigation tool as it allows for extracting information, which would otherwise require two independent experiments, i.e., absorption and luminescence.

In Fig. 2 (top) we show the evolution of the k-resolved electron density in the conduction band. At time $t = 0$ the profile is proportional to the square of the exciton wave function in momentum space, i.e., $n_k^c(0) \propto |Y_k^{(x)}|^2$, see Appendix A. As time increases the exciton transforms into an exciton-polaron and the wave function slightly spreads. Thus the dressed *eh* wave packet becomes more localized in real-space, in agreement with the larger binding energy observed in Fig. 1 (middle). We observe that the phonon dressing occurs on a much faster time-scale than the decoherence time, i.e., the timescale over which the polarization damps. This can also be seen from the plot of the time-dependent standard deviation $\sigma_Q(t)$, see Fig. 2 (bottom). According to Eq. (C9) the

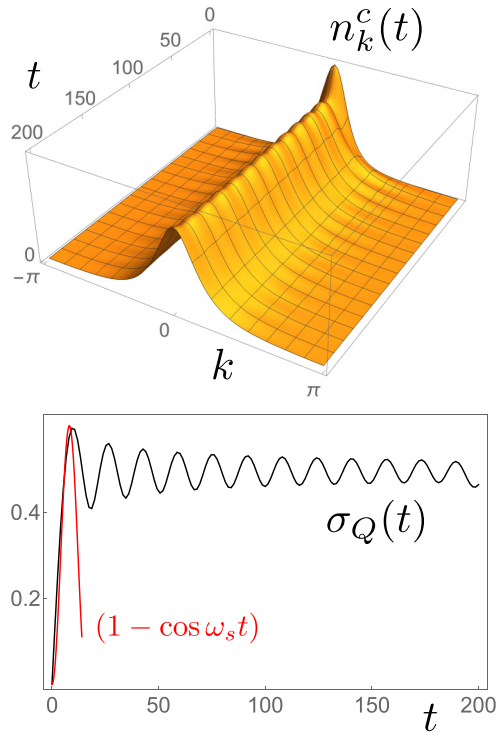

FIG. 2. Top: Time-dependent k-resolved electronic occupations in the conduction band. Bottom: Time-dependent standard deviation of the phonon momentum.

standard deviation grows like $\sigma_Q(t) \propto (1-\cos\omega_s t)$. Hence the timescale $\tau_{\rm dress}$ for the phonon dressing is

$$\tau_{\rm dress} = \frac{2\pi}{\omega_s} \simeq 16.3. \tag{50}$$

The envelope function of the polarization can be found from Eq. (49). After some simple algebra one finds an approximate exponential decay $\exp[-t/\tau_{\rm decoh}]$ with decoherence time

$$\tau_{\rm decoh} = \frac{\omega_s}{2\lambda_0^2} = 23.8. \tag{51}$$

In Fig. 1 (right) the envelope function nicely interpolates all maxima of the time-dependent polarization, see red curve. We emphasize that the dressing time is dictated by the largest phonon frequency whereas the decoherence time is dictated by the smallest polaronic shift. Furthermore, the dressing timescale does not appear in an exponential function, see again Fig. 2. We also notice that $\sigma_Q(t) \simeq 0.5$ in the long-time limit; hence, similar results would have been obtained for a dispersive conduction band with a shallow enough minimum.

Although the electronic occupations as well as the polarization attain a steady value in the long time limit the phononic occupations do not. This behavior is a direct consequence of the acoustic dispersion and the low dimensionality. In Appendix C we demonstrate that $n_q(t) = |f_q(t)|^2$ where the function $f_q(t)$ is given in Eq. (42). Therefore the total number of phonons at time t is given by $N_{\rm ph}(t) = \frac{2}{\mathcal{N}}\sum_q (\frac{\lambda_q}{\omega_q})^2(1-\cos\omega_q t)$. For large times the main contribution to the sum comes from low-momentum phonons. Approximating $\omega_q \simeq \omega_s|q|$, $\lambda_q \simeq \lambda_0$ and taking the thermodynamic limit $\mathcal{N}\to\infty$ we then find

$$N_{\rm ph}(t) \simeq \frac{\lambda_0^2}{\omega_s}\, t = \frac{1}{2}\frac{t}{\tau_{\rm decoh}}. \tag{52}$$

Thus the total number of phonons increases linearly in time. It is easy to show that the divergence of $N_{\rm ph}(t)$ as $t\to\infty$ is milder in two dimensions, being it $\log(t)$, and it is absent in three dimensions. We also observe that the free-phonon contribution to the total energy $E_{\rm ph}(t) = \sum_q \omega_q n_q(t)$ diverges like $\log(t)$ in one dimension whereas it approaches a constant value for larger dimensions.

V. NONRESONANT PUMPING

Electrons pumped in the conduction band have enough energy to emit optical phonons and hence to decay into a bound exciton state. The issue we intend to address here is whether the spectral function exhibits an excitonic structure inside the gap and, in the affirmative case, what the shape is.

As already pointed out the exact solution of the two-band model Hamiltonian does not attain a steady state for optical phonons, see discussion in Sec. III A. However, probing the system with pulses of duration much longer than the inverse of the phonon frequency the spectral function $A_k(T,\omega)$ becomes independent of T as $T\to\infty$. We consider again a 1D model with a flat conduction band and a dispersive valence band separated by an energy gap E_g: $\epsilon_k^c = \epsilon_c = E_g/2$ (CBM at $E_g/2$) and $\epsilon_k^v = E_g[\cos k - 1] - E_g/2$ (VBM at $-E_g/2$). We also consider the same short-range Coulomb interaction $U_p = 0.65$ (all energies are in units of E_g) as in the previous section—hence the system admits one exciton state at energy $E^{(\rm x)} = 0.81$. Let us assume that the pump has excited the system in a wave packet of continuum eh states $\mathbf{Y}^{(c)}$ of the Bethe-Salpeter Hamiltonian $\mathbb{H}$ with energy $E^{(c)} \simeq E_g$, hence

$$\mathbf{Y}^0 = \frac{1}{\sqrt{\mathcal{N}_0}} \sum_{c:E^{(c)}\simeq E_g} \mathbf{Y}^{(c)}, \tag{53}$$

where $\mathcal{N}_0$ is the number of eigenstates in the sum. In the thermodynamic limit the ratio $r_0 = \mathcal{N}_0/\mathcal{N} \ll 1$ remains finite. At zero pump-probe delay, i.e., $T=0$, we can ignore phonon effects and the spectral function reads [compare with the resonant case Eq. (48)]:

$$A_k(0,\omega) = 2\pi|\beta|^2 \left|Y_k^0\right|^2 \delta(\omega - E_g/2). \tag{54}$$

As Y_k^0 is peaked around $k=0$ the spectral function $A_{k\simeq 0}(0,\omega)$ is peaked at frequency $\omega \simeq E_g/2 = \epsilon^c$ (CBM), and it is vanishingly small for nonvanishing momenta.

In Appendix A we show that for electrons coupled to a branch of optical phonons of frequency ω_0 the spectral function in the long-time limit becomes

$$\lim_{T\to\infty} A_k(T,\omega) = \lim_{T\to\infty}\frac{|\beta|^2}{T} \times \Big\{ \left|\tilde{Y}_{k0}\left(\omega-\epsilon_k^v\right)\right|^2 + \sum_{M=1}^{\infty}\frac{1}{\mathcal{N}}\sum_p \left|\tilde{Y}_{pM}\left(\omega-\epsilon_p^v+M\omega_0\right)\right|^2 \Big\}. \tag{55}$$

The amplitudes $\tilde{\mathbf{Y}}_M(\omega)$ are the Fourier transform of the time-dependent amplitudes $\mathbf{Y}_M(t)$ in Eq. (31). Interestingly only the first term ($M = 0$) depends on k. All remaining terms ($M \geqslant 1$) contribute with a k-independent function of the frequency (a consequence of the nondispersive nature of the conduction band). Expanding the amplitudes like in Eq. (34) we can equivalently calculate $\tilde{\mathbf{Y}}_M(\omega)$ from the Fourier transform of the hierarchy in Eq. (35). We neglect here the couplings $L_{cc'}$ between low-energy continuum states since these scatterings are suppressed by energy conservation. We instead consider the couplings $L_{\rm cx} = L_{\rm xc} = \lambda_0/\sqrt{\mathcal{N}}$ between the exciton state and the continuum states. We then find

$$i\dot{\alpha}_{cM} = (E^{(c)} + M\omega_0)\alpha_{cM} + \frac{\lambda_0}{\sqrt{\mathcal{N}}}[\sqrt{M}\alpha_{{\rm x}M-1} + \sqrt{M+1}\alpha_{{\rm x}M+1}], \quad (56)$$

$$i\dot{\alpha}_{{\rm x}M} = (E^{({\rm x})} + M\omega_0)\alpha_{{\rm x}M} + \frac{\lambda_0}{\sqrt{\mathcal{N}}}\sum_c[\sqrt{M}\alpha_{cM-1} + \sqrt{M+1}\alpha_{cM+1}], \quad (57)$$

to be solved with boundary conditions $\alpha_{cM}(0) = \delta_{M0}/\sqrt{\mathcal{N}_0}$ if $E^{(c)} \simeq E_g$ and zero otherwise, see Eq. (53). The symmetry of the electron-phonon coupling preserves the symmetry of the initial state, i.e., $\alpha_{cM}(t)$ is independent of c if $E^{(c)} \simeq E_g$ and $\alpha_{cM}(t) = 0$ otherwise. We can therefore simplify the hierarchy by introducing the quantity $\alpha_{CM}(t) = \sum_c \alpha_{cM}(t)$ and by taking into account that $E^{(c)} \simeq E_g$ for all c in the initial wave packet. To gain some insight we solve the simplified hierarchy to lowest order in λ_0, i.e., we neglect processes with the emission of two or more phonons. These processes are relevant for strong electron-phonon coupling and give rise to phononic replica bands [63–69]. Fourier transforming Eqs. (56) and (57) we find

$$\tilde{\alpha}_{C0}(\omega) = -\frac{1}{\sqrt{\mathcal{N}_0}}\,{\rm Im}\left[\frac{1}{\omega - E_g - \frac{r_0\lambda_0^2}{\omega - E^{({\rm x})} - \omega_0}}\right], \quad (58)$$

$$\tilde{\alpha}_{{\rm x}1}(\omega) = -\lambda_0 r_0\,{\rm Im}\left[\frac{1}{(\omega - E_g - r_0\lambda_0^2)(\omega - E^{({\rm x})} - \omega_0)}\right], \quad (59)$$

and $\tilde{\alpha}_{C1}(\omega) = \tilde{\alpha}_{{\rm x}0} = 0$. Using these solutions the asymptotic spectral function of Eq. (55) becomes

$$\lim_{T\to\infty} A_k(T,\omega) = \lim_{T\to\infty}\frac{|\beta|^2}{T}\left\{\left|\tilde{\alpha}_{C0}(\omega + E_g/2)Y_k^0\right|^2 + \frac{1}{\mathcal{N}}\sum_p\left|\tilde{\alpha}_{{\rm x}1}\left(\omega - \epsilon_p^v + \omega_0\right)Y_p^{({\rm x})}\right|^2\right\}. \quad (60)$$

In Fig. 3 we show the spectral function for a system with $\mathcal{N} = 501$ k-points, $r_0 = 0.05$ and phonon frequency $\omega_0 = E_g - E^{\rm x} \simeq 0.2$. In the weak coupling regime $\lambda_0 = 0.02$ (top panel) the quasiparticle peak at the CBM (frequency $\omega = E_g/2$, black curve) is accompanied by an excitonic structure (blue curve) having asymmetric lineshape and offset at frequency $\omega \simeq E^{({\rm x})}$. The main effect of an increased electron-phonon coupling is the splitting of the quasiparticle peak

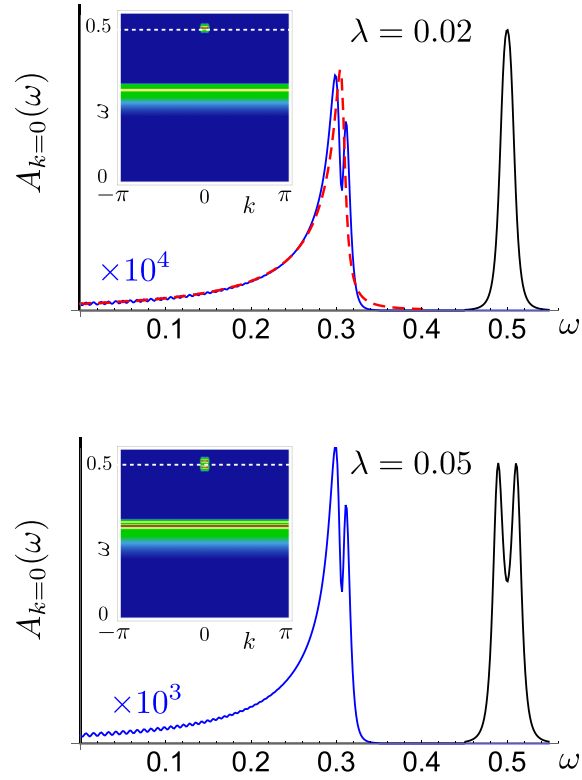

FIG. 3. Spectral function $A_{k\simeq 0}(\omega)$ in the long-time limit $T \to \infty$ for a weak ($\lambda_0 = 0.02$, top panel) and intermediate ($\lambda_0 = 0.05$, bottom panel) electron-phonon coupling. The exciton contribution (blue line) is magnified by a factor 10^4 (top) and 10^3 (bottom). The dashed (red) line in the top panel is the exciton wave function in energy space, see main text. The insets show the color plot of the spectral function in the $k - \omega$ plane.

(energy splitting $\simeq \lambda_0^2 r_0$) and a larger intensity of the excitonic structure, see bottom panel.

In both (weak and intermediate) regimes the momentum and energy dispersion of the excitonic structure is considerably different from the resonant case, compare insets of Fig. 3 with left and middle panels of Fig. 1. We point out that this marked qualitative difference is not related to the phonon dispersion. For resonant pumping a replica of the valence band would have emerged even with optical phonons. The results in Fig. 3 clearly indicate that incoherent excitons forming after nonresonant pumping give rise to a replica of the *conduction* band, thus confirming the nonequilibrium T-matrix Green's function treatment [20,21,48].

It is also worth commenting on the asymmetric lineshape at fixed k (blue line) of the excitonic structure. This feature too was observed in the nonequilibrium T-matrix Green's function treatment [20,21]. The exact solution allows for a precise characterization of it. The excitonic sideband originates from the second term in Eq. (60). Taking into account the explicit form of $\tilde{\alpha}_{{\rm x}1}(\omega)$ in Eq. (59) we see that the asymmetric lineshape is well described by $\mathcal{L}(\omega) \equiv \sum_p \delta(\omega - E^{({\rm x})} - \epsilon_p^v)|Y_p^{({\rm x})}|^2$. The function $\mathcal{L}$ is shown in the top panel of Fig. 3 (dashed line) and it can be interpreted as the excitonic wave function in "energy space".

VI. SUMMARY

We have calculated the trARPES spectra of a two-band model semiconductor with a flat conduction band from the analytic solution of the time-dependent many-body wave function. Both electron-electron and electron-phonon interactions have been taken into account, and the exact solution has been worked out for acoustic as well as optical phonons. Numerical results have been presented to address open issues on the spectra of resonantly and nonresonantly excited semiconductors after phonon-induced decoherence and relaxation.

In resonantly excited semiconductor the initial excitonic sideband is a replica of the valence band located at the onset of the photoabsorption spectrum (with respect to the VBM). After phonon-induced decoherence the excitonic sideband changes slightly but it does not fade away. In particular its position is red-shifted (Stokes shift) ending up at the onset of the photoluminescence spectrum (with respect to the VBM). Phonon-dressing is also responsible for a broadening of the sideband, in agreement with the transition from excitons to exciton-polarons. We also find that phonon dressing occurs on a much faster time-scale than phonon-induced decoherence, the former being dictated by the largest phonon frequency whereas the latter by the smallest polaronic shift. In the incoherent phase the electronic subsystem is in a stationary state, i.e., the electronic occupations and the electronic Green's function are invariant under time translations. The stationarity of the phononic subsystem does instead depend on the dimensionality; the number of low-momentum acoustic phonons grows in time linearly in one-dimension, logarithmically in two dimensions and attains a constant value in larger dimensions.

In nonresonantly excited semiconductor the excitonic sideband forms only after phonon-driven relaxation. Its shape is a replica of the conduction band and its energy distribution at fixed momentum has a highly asymmetric lineshape. The lineshape is proportional to the exciton wave function in energy space.

The considered two-band model ignores several aspects of real materials, e.g., multiple bands and valleys, intraband and interband long-range Coulomb interactions, band anisotropies and degeneracies, multiple phonon branches, etc. [70]. However, the addressed issues are independent of these details. In Ref. [23] we have shown that the excitonic features of the ARPES spectrum of a bulk LiF in the resonant phase could be predicted using the same model. The scenario emerging from our exact solution is therefore expected to be generally applicable to the interpretation of experimental trARPES spectra.

ACKNOWLEDGMENTS

We acknowledge the financial support from MIUR PRIN (Grant No. 20173B72NB), from INFN through the TIME2QUEST project, and from Tor Vergata University through the Beyond Borders Project ULEXIEX.

APPENDIX A: CONDUCTION-CONDUCTION GREEN'S FUNCTION

Let us begin with the calculation of the conduction-conduction Green's function defined in Eq. (12). For convenience we rewrite it as

$$G_k^{cc}(t,t') = i|\beta|^2 \rho_k^{cc}(t,t'), \tag{A1}$$

where $\rho_k^{cc}(t,t') \equiv \langle \Phi_x(t')|\hat{c}_k^\dagger e^{-i\hat{H}(t'-t)}\hat{c}_k|\Phi_x(t)\rangle$. Using the expansion in Eq. (19) we have

$$\rho_k^{cc}(t,t') = \sum_{pp'}\sum_{M=0}^{\infty}\frac{1}{(M!)^2}\sum_{\substack{q_1\dots q_M\\ q_1'\dots q_M'}} Y^*_{p'q_1'\dots q_M'}(t')Y_{pq_1\dots q_M}(t)\langle p'q_1'\dots q_M'|\hat{c}_k^\dagger e^{-i\hat{H}(t'-t)}\hat{c}_k|pq_1\dots q_M\rangle. \tag{A2}$$

For vanishing electron-phonon coupling $Y_k(t) = Y_k^0(t)$ and $Y_{pq_1\dots q_M}(t) = 0$ for all $M \geqslant 1$. We thus recover the purely electronic result

$$\rho_k^{0cc}(t,t') \equiv \lim_{\{\lambda_q^k\}\to 0}\rho_k^{cc}(t,t') = e^{i\epsilon_k^v(t'-t)}Y_k^{0*}(t')Y_k^0(t). \tag{A3}$$

If the initial state $\mathbf{Y}^0$ is an eigenstate $\mathbf{Y}^{(\mu)}$ of $\mathbb{H}$ with energy $E^{(\mu)}$ then $Y_k^0(t) = Y_k^{(\mu)}e^{-iE^{(\mu)}t}$ and Eq. (A3) becomes

$$\rho_k^{0cc}(t,t') = \left|Y_k^{(\mu)}\right|^2 e^{-i(\epsilon_k^v+E^{(\mu)})(t-t')}. \tag{A4}$$

In this case the spectral function $A_k(T,\omega)$ in Eq. (14) is independent of T and for each k it exhibits a single peak at energy $\epsilon_k^v + \epsilon^{(\mu)}$:

$$A_k(T,\omega) = 2\pi|\beta|^2\left|Y_k^{(\mu)}\right|^2\delta(\omega-\epsilon_k^v-E^{(\mu)}). \tag{A5}$$

To proceed with the calculation of the Green's function of the coupled electron-phonon system we observe that the state $\hat{c}_k|pq_1\dots q_M\rangle$ in Eq. (A2) is a state with no electrons in the conduction band and with a hole of momentum p in the valence band. Therefore

$$e^{i\hat{H}\tau}\hat{c}_k|pq_1\dots q_M\rangle = e^{i(-\epsilon_p^v+\omega_{q_1}\dots+\omega_{q_M})\tau}\hat{c}_k|pq_1\dots q_M\rangle. \tag{A6}$$

Furthermore

$$\langle p'q'_1 \dots q'_M | \hat{c}^\dagger_k \hat{c}_k | p q_1 \dots q_M \rangle = \delta_{p'p} \sum_P \prod_{j=1}^M \delta_{q'_j q_{P(j)}} \delta_{k,p-q_1\dots-q_M}. \tag{A7}$$

1. *q*-independent coupling

We insert Eqs. (A6) and (A7) into Eq. (A2) and use the solution in Eq. (30) for the amplitudes. We find

$$\begin{aligned}\rho^{cc}_k(t,t') &= \sum_{q_1\dots q_M} \delta_{k,p-q_1\dots-q_M} \\ &\quad \times \sum_p \sum_{M=0}^\infty \frac{1}{\mathcal{N}^M} Y^*_{pM}(t') Y_{pM}(t) e^{i(\epsilon^v_p - M\omega_0)(t'-t)} \\ &= Y^*_{k0}(t') Y_{k0}(t) e^{i\epsilon^v_k (t'-t)} \\ &\quad + \frac{1}{\mathcal{N}} \sum_p \sum_{M=1}^\infty Y^*_{pM}(t') Y_{pM}(t) e^{i(\epsilon^v_p - M\omega_0)(t'-t)}. \end{aligned} \tag{A8}$$

For vanishing electron-phonon coupling only the first term on the right hand side contributes and we recover Eq. (A3).

Let us study the steady-state limit of Eq. (A8). We define the center-of-mass time $T = (t + t')/2$ and the relative time $\tau = (t - t')$. Given a function $a(t)$ with Fourier transform $\tilde{a}(\omega)$ we have

$$\begin{aligned}\lim_{T\to\infty} a(t) a^*(t') &= \int \frac{d\omega}{2\pi} e^{-i\omega\tau} \lim_{T\to\infty} \int \frac{d\Omega}{2\pi} e^{-i\Omega T} \\ &\quad \times \tilde{a}\left(\omega + \frac{\Omega}{2}\right) \tilde{a}^*\left(\omega - \frac{\Omega}{2}\right) \\ &= \lim_{T\to\infty} \frac{1}{T} \int \frac{d\omega}{2\pi} e^{-i\omega\tau} |\tilde{a}(\omega)|^2, \end{aligned} \tag{A9}$$

where in the last equality we used the Riemann-Lebesgue theorem. Using this result in Eq. (A8) with functions $a(t) = Y_{pM}(t) e^{-i(\epsilon^v_p - M\omega_0)t}$ and taking into account Eq. (14) for the spectral function we find Eq. (55).

2. *k*-independent coupling

Proceeding along the same lines as for the q-independent coupling but using the solution in Eq. (45) we find

$$\begin{aligned}\rho^{cc}_k(t,t') &= \sum_p e^{i\epsilon^v_p (t'-t)} Y^{0*}_p(t') Y^0_p(t) \ell^*(t') \ell(t) \sum_M \frac{1}{M!} \\ &\quad \times \sum_{q_1\dots q_M} \delta_{k,p-q_1\dots-q_M} \prod_{j=1}^M f^*_{q_j}(t') f_{q_j}(t) e^{-i\omega_{q_j}(t'-t)}. \end{aligned} \tag{A10}$$

We define the function

$$h_q(t,t') \equiv f^*_q(t') f_q(t) e^{-i\omega_q (t'-t)}, \tag{A11}$$

and its Fourier expansion

$$h_q(t,t') = \sum_n e^{iqn} \frac{\tilde{h}_n(t,t')}{\mathcal{N}}. \tag{A12}$$

Depending on the dimensionality D of the system the product $qn \equiv \sum_{i=1}^D q_i n_i$ stands for the scalar product between the vector q in the first Brillouin zone and the position n of the unit cell. The domain over which n runs is such that $\frac{1}{\mathcal{N}} \sum_n e^{i(q-q')n} = \delta_{qq'}$ and $\frac{1}{\mathcal{N}} \sum_q e^{iq(n-n')} = \delta_{nn'}$. We can then use the identity

$$\sum_{q_1\dots q_M} \delta_{k,p-q_1\dots-q_M} \prod_{j=1}^M h_{q_j}(t,t') = \sum_n e^{i(p-k)n} \frac{[\tilde{h}_n(t,t')]^M}{\mathcal{N}} \tag{A13}$$

to perform the sum over M in Eq. (A10), obtaining the following compact expression

$$\rho^{cc}_k(t,t') = \sum_p K_{k-p}(t,t')\, e^{i\epsilon^v_p (t'-t)} Y^{0*}_p(t') Y^0_p(t). \tag{A14}$$

In Eq. (A14) the kernel

$$K_{k-p}(t,t') \equiv \ell^*(t') \ell(t) \frac{1}{\mathcal{N}} \sum_n e^{i(p-k)n} e^{\tilde{h}_n(t,t')} \tag{A15}$$

is the only quantity depending on the electron-phonon couplings and phonon frequencies.

For vanishing electron-phonon coupling, i.e., $\lambda_q = 0$ for all q, the Langreth function $\ell(t) = 1$, see Eq. (40), and the function $\tilde{h}_n(t,t') = 0$. Therefore

$$K^0_{k-p}(t,t') \equiv \lim_{\{\lambda_q\}\to 0} K_{k-p}(t,t') = \delta_{kp} \tag{A16}$$

and Eq. (A14) correctly reduces to the purely electronic result in Eq. (A3). The conduction-conduction Green's function of the interacting electron-phonon system is a convolution in momentum space between the Green's function of the purely electronic system ρ^{0cc} and the kernel K. Indeed Eq. (A14) can be rewritten as

$$\rho^{cc}_k(t,t') = \sum_p K_{k-p}(t,t') \rho^{0cc}_p(t,t'). \tag{A17}$$

For the system to attain a steady state in the long-time limit the kernel $K_{k-p}(t,t')$ has to approach a function of $\tau = t - t'$ for $t, t' \to \infty$. If we denote by $K_{k-p}(\omega)$ its Fourier transform then the steady-state spectral function in Eq. (14) reads

$$\lim_{T\to\infty} A_k(T,\omega) = \sum_p \int \frac{d\omega'}{2\pi} K_{k-p}(\omega - \omega') A^0_p(\omega'), \tag{A18}$$

where $A^0_p(\omega')$ is the spectral function of the purely electronic system.

APPENDIX B: CONDUCTION-VALENCE GREEN'S FUNCTION

The calculation of the off-diagonal Green's function in Eq. (13) is straightforward. We start by rewriting it as

$$G^{cv}_k(t,t') = i\alpha^* \beta \rho^{cv}_k(t,t'), \tag{B1}$$

where $\rho_k^{cv}(t,t') \equiv \langle\Phi_0|\hat{v}_k^\dagger e^{-i\hat{H}(t'-t)}\hat{c}_k|\Phi_x(t)\rangle$. Inserting the expansion in Eq. (19) and using Eq. (A6) we find

$$\rho_k^{cv}(t,t') = \sum_p \sum_{M=0}^{\infty} \frac{1}{M!} \sum_{q_1\ldots q_M} Y_{pq_1\ldots q_M}(t) \times e^{i(\epsilon_p^v - \omega_{q_1}\ldots-\omega_{q_M})(t'-t)}\langle\Phi_0|\hat{v}_k^\dagger\hat{c}_k|pq_1\ldots q_M\rangle. \tag{B2}$$

The bracket in this equation is nonvanishing only for $M=0$ and $k=p$, in which case its value is unity. Hence

$$\rho_k^{cv}(t,t') = Y_k(t)e^{i\epsilon_k^v(t'-t)}. \tag{B3}$$

For k-independent coupling this result further simplifies since $Y_k(t) = \ell(t)Y_k^0(t)$, see Eq. (45).

APPENDIX C: TIME-DEPENDENT PHONON OCCUPATIONS AND MOMENTUM DISTRIBUTION

The time-dependent phonon occupancy is defined in Eq. (10). Taking into account the expansion in Eq. (19) we have

$$n_q(t) = \sum_{M=0}^{\infty}\frac{1}{(M!)^2}\sum_{kk'}\sum_{\substack{q_1\ldots q_M\\ q_1'\ldots q_M'}} Y^*_{k'q_1'\ldots q_M'}(t) \times Y_{kq_1\ldots q_M}(t)\langle k'q_1'\ldots q_M'|\hat{b}_q^\dagger\hat{b}_q|kq_1\ldots q_M\rangle. \tag{C1}$$

From the inner product in Eq. (20) it follows that

$$\langle k'q_1'\ldots q_M'|\hat{b}_q^\dagger\hat{b}_q|kq_1\ldots q_M\rangle = \delta_{k'k}\sum_P\prod_{j=1}^M\delta_{q_j'q_{P(j)}}\sum_{j=1}^M\delta_{qq_j}. \tag{C2}$$

Using the total symmetry of the amplitudes we then get

$$n_q(t) = \sum_{M=0}^{\infty}\frac{1}{M!}\sum_{k,q_1\ldots q_M}\sum_{j=1}^M\delta_{qq_j}|Y_{kq_1\ldots q_M}(t)|^2. \tag{C3}$$

We are also interested in the phonon-momentum distribution. The phonon-momentum operator is given by $\hat{Q} = \sum_q q\,\hat{n}_q$. The average momentum of the exciton-polaron state is therefore

$$Q(t) = \langle\Phi_x(t)|\hat{Q}|\Phi_x(t)\rangle = \sum_{M=0}^{\infty}\frac{1}{M!}\sum_{k,q_1\ldots q_M}\sum_{j=1}^M q_j|Y_{kq_1\ldots q_M}(t)|^2, \tag{C4}$$

whereas the standard deviation is

$$\sigma_Q^2(t) = \langle\Phi_x(t)|\hat{Q}^2|\Phi_x(t)\rangle - Q^2(t) = \sum_{M=0}^{\infty}\frac{1}{M!}\sum_{k,q_1\ldots q_M}\sum_{ij=1}^M q_iq_j|Y_{kq_1\ldots q_M}(t)|^2 - Q^2(t). \tag{C5}$$

The condition in Eq. (26) is satisfied provided that $Q(t)\simeq 0$ and $\sigma_Q(t)$ is much smaller than the momentum-scale over which the conduction band changes.

1. q-independent coupling

Let us evaluate Eq. (C3) using the solution of Eq. (30) for q-independent couplings. It is straightforward to find

$$n_q(t) = \sum_{M=0}^{\infty} M \times \sum_k \frac{|Y_{kM}(t)|^2}{\mathcal{N}}. \tag{C6}$$

Hence the phonon occupancy depends on the initial electronic state $\mathbf{Y}^0$ but it does not depend of q (all modes are equally populated). This implies that $Q(t)=0$ and hence the standard deviation is simply

$$\sigma_Q^2(t) = \sum_q q^2\sum_{M=0}^{\infty} M \times \sum_k \frac{|Y_{kM}(t)|^2}{\mathcal{N}}. \tag{C7}$$

2. k-independent coupling

For k-independent couplings we substitute the solution of Eq. (45) and find

$$n_q(t) = \sum_{M=0}^{\infty}\frac{1}{M!}M|f_q(t)|^2\left(\sum_{q'}|f_{q'}(t)|^2\right)^{M-1}|\ell(t)|^2 = |f_q(t)|^2, \tag{C8}$$

where we have taken into account that $\sum_k|Y_k^0(t)|^2 = \mathbf{Y}^{0\dagger}e^{i\mathbb{H}t}e^{-i\mathbb{H}t}\mathbf{Y}^0 = 1$. In this case the phonon occupancy in Eq. (C8) is *independent* of the initial state.

Assuming that $f_q(t) = f_{-q}^*(t)$ the average momentum $Q(t)=0$ for all times. Therefore the standard deviation reads

$$\sigma_Q^2(t) = \sum_q q^2|f_q(t)|^2. \tag{C9}$$

[1] A. Damascelli, Z. Hussain, and Z.-X. Shen, Rev. Mod. Phys. **75**, 473 (2003).
[2] I. M. Vishik, Rep. Prog. Phys. **81**, 062501 (2018).
[3] S. Doniach and M. Sunjic, J. Phys. C: Solid State Phys. **3**, 285 (1970).
[4] P. H. Citrin, G. K. Wertheim, and Y. Baer, Phys. Rev. B **16**, 4256 (1977).
[5] S. Hüfner, *Photoelectron Spectroscopy* (Springer, Berlin, 2003).
[6] K. Rossnagel, Synchrotron Radiation News **25**, 12 (2012).
[7] D. Sangalli and A. Marini, Europhys. Lett. **110**, 47004 (2015).
[8] C. L. Smallwood, R. A. Kaindl, and A. Lanzara, Europhys. Lett. **115**, 27001 (2016).
[9] S.-K. Mo, Nano Convergence **4**, 6 (2017).
[10] F. Caruso, D. Novko, and C. Draxl, Phys. Rev. B **101**, 035128 (2020).
[11] B. Lv, T. Qian, and H. Ding, Nat. Rev. Phys. **1**, 609 (2019).
[12] Y. Wakisaka, T. Sudayama, K. Takubo, T. Mizokawa, M. Arita, H. Namatame, M. Taniguchi, N. Katayama, M. Nohara, and H. Takagi, Phys. Rev. Lett. **103**, 026402 (2009).

[13] K. Seki, Y. Wakisaka, T. Kaneko, T. Toriyama, T. Konishi, T. Sudayama, N. L. Saini, M. Arita, H. Namatame, M. Taniguchi *et al.*, Phys. Rev. B **90**, 155116 (2014).

[14] M. Dendzik, R. P. Xian, E. Perfetto, D. Sangalli, D. Kutnyakhov, S. Dong, S. Beaulieu, T. Pincelli, F. Pressacco, D. Curcio *et al.*, Phys. Rev. Lett. **125**, 096401 (2020).

[15] M. Weinelt, M. Kutschera, T. Fauster, and M. Rohlfing, Phys. Rev. Lett. **92**, 126801 (2004).

[16] T. Suzuki and R. Shimano, Phys. Rev. Lett. **103**, 057401 (2009).

[17] X.-Y. Zhu, J. Electron. Spectrosc. Relat. Phenom. **204**, 75 (2015).

[18] E. Varene, L. Bogner, C. Bronner, and P. Tegeder, Phys. Rev. Lett. **109**, 207601 (2012).

[19] J.-C. Deinert, D. Wegkamp, M. Meyer, C. Richter, M. Wolf, and J. Stähler, Phys. Rev. Lett. **113**, 057602 (2014).

[20] E. Perfetto, D. Sangalli, A. Marini, and G. Stefanucci, Phys. Rev. B **94**, 245303 (2016).

[21] A. Steinhoff, M. Florian, M. Rösner, G. Schönhoff, T. O. Wehling, and F. Jahnke, Nat. Commun. **8**, 1166 (2017).

[22] A. Rustagi and A. F. Kemper, Phys. Rev. B **97**, 235310 (2018).

[23] E. Perfetto, D. Sangalli, A. Marini, and G. Stefanucci, Phys. Rev. Materials **3**, 124601 (2019).

[24] D. Christiansen, M. Selig, E. Malic, R. Ernstorfer, and A. Knorr, Phys. Rev. B **100**, 205401 (2019).

[25] X. Jun, Z. Mervin, W. Yuan, and Z. Xiang, Nanoph. **6**, 1309 (2017).

[26] T. Östreich and K. Schönhammer, Z. Phys. B **91**, 189 (1993).

[27] K. Hannewald, S. Glutsch, and F. Bechstedt, J. Phys.: Condens. Matter **13**, 275 (2000).

[28] M. H. Szymańska, J. Keeling, and P. B. Littlewood, Phys. Rev. Lett. **96**, 230602 (2006).

[29] R. Hanai, P. B. Littlewood, and Y. Ohashi, J. Low Temp. Phys. **183**, 127 (2016).

[30] R. Hanai, P. B. Littlewood, and Y. Ohashi, Phys. Rev. B **96**, 125206 (2017).

[31] K. W. Becker, H. Fehske, and V.-N. Phan, Phys. Rev. B **99**, 035304 (2019).

[32] D. Kremp, D. Semkat, and K. Henneberger, Phys. Rev. B **78**, 125315 (2008).

[33] E. Perfetto, S. Bianchi, and G. Stefanucci, Phys. Rev. B **101**, 041201(R) (2020).

[34] K. Hannewald, S. Glutsch, and F. Bechstedt, Phys. Rev. B **62**, 4519 (2000).

[35] Y. Murakami, M. Schüler, S. Takayoshi, and P. Werner, Phys. Rev. B **101**, 035203 (2020).

[36] S. K. Sundaram and E. Mazur, Nat. Mater. **1**, 217 (2002).

[37] L. Bányai, D. B. Tran Thoai, E. Reitsamer, H. Haug, D. Steinbach, M. U. Wehner, M. Wegener, T. Marschner, and W. Stolz, Phys. Rev. Lett. **75**, 2188 (1995).

[38] S. Bar-Ad and D. Chemla, Mater. Sci. Eng., B **48**, 83 (1997).

[39] D. Sangalli and A. Marini, J. Phys.: Conf. Ser. **609**, 012006 (2015).

[40] M. Palummo, M. Bernardi, and J. C. Grossman, Nano Lett. **15**, 2794 (2015).

[41] G. Wang, A. Chernikov, M. M. Glazov, T. F. Heinz, X. Marie, T. Amand, and B. Urbaszek, Rev. Mod. Phys. **90**, 021001 (2018).

[42] M. K. L. Man, J. Madèo, C. Sahoo, K. Xie, M. Campbell, V. Pareek, A. Karmakar, E. L. Wong, A. Al-Mahboob, N. S. Chan *et al.*, Sci. Adv. **7**, eabg0192 (2020).

[43] S. Dong, M. Puppin, T. Pincelli, S. Beaulieu, D. Christiansen, H. Hubener, C. W. Nicholson, R. P. Xian, M. Dendzik, Y. Deng *et al.*, arXiv:2012.15328.

[44] Y. Toyozawa, *Quantum Statistics of Charged Particle Systems* (Plenum, New York, 1986).

[45] R. Schepe, T. Schmielau, D. Tamme, and K. Henneberger, Phys. Status Solidi B **206**, 273 (1998).

[46] C. Piermarocchi and F. Tassone, Phys. Rev. B **63**, 245308 (2001).

[47] N. H. Kwong, G. Rupper, and R. Binder, Phys. Rev. B **79**, 155205 (2009).

[48] K. Asano and T. Yoshioka, J. Phys. Soc. Jpn. **83**, 084702 (2014).

[49] Y. Toyozawa, *Optical Processes in Solids* (Cambridge University Press, Cambridge, 2003).

[50] M. Hohenadler, P. B. Littlewood, and H. Fehske, Phys. Rev. B **76**, 184303 (2007).

[51] E. Burovski, H. Fehske, and A. S. Mishchenko, Phys. Rev. Lett. **101**, 116403 (2008).

[52] H. Haug and S. W. Koch, *Quantum Theory of the Optical and Electronic Properties of Semiconductors* (World Scientific, Singapore, 1994).

[53] W. Schäfer and M. Wegener, *Semiconductor Optics and Transport Phenomena* (Springer-Verlag, Berlin, 2002).

[54] D. F. Martinez, J. Phys. A **36**, 9827 (2003).

[55] G. Stefanucci, S. Kurth, A. Rubio, and E. K. U. Gross, Phys. Rev. B **77**, 075339 (2008).

[56] D. C. Langreth, Phys. Rev. B **1**, 471 (1970).

[57] S. Schmitt-Rink, D. S. Chemla, and H. Haug, Phys. Rev. B **37**, 941 (1988).

[58] W. Schäfer and J. Treusch, Z. Phys. B **63**, 407 (1986).

[59] M. Lindberg and S. W. Koch, Phys. Rev. B **38**, 3342 (1988).

[60] E. Perfetto and G. Stefanucci, Phys. Rev. Lett. **125**, 106401 (2020).

[61] S. Li, J. Luo, J. Liu, and J. Tang, J. Phys. Chem. Lett. **10**, 1999 (2019).

[62] W. Hoyer, C. Ell, M. Kira, S. W. Koch, S. Chatterjee, S. Mosor, G. Khitrova, H. M. Gibbs, and H. Stolz, Phys. Rev. B **72**, 075324 (2005).

[63] S. Moser, L. Moreschini, J. Jaćimović, O. S. Barišić, H. Berger, A. Magrez, Y. J. Chang, K. S. Kim, A. Bostwick, E. Rotenberg *et al.*, Phys. Rev. Lett. **110**, 196403 (2013).

[64] S. M. Story, J. J. Kas, F. D. Vila, M. J. Verstraete, and J. J. Rehr, Phys. Rev. B **90**, 195135 (2014).

[65] C. Chen, J. Avila, E. Frantzeskakis, A. Levy, and M. C. Asensio, Nat. Commun. **6**, 8585 (2015).

[66] G. Antonius, S. Poncé, E. Lantagne-Hurtubise, G. Auclair, X. Gonze, and M. Côté, Phys. Rev. B **92**, 085137 (2015).

[67] Z. Wang, S. M. Walker, A. Tamai, Y. Wang, Z. Ristic, F. Y. Bruno, A. De La Torre, S. Riccò, N. Plumb, M. Shi *et al.*, Nat. Mater. **15**, 835 (2016).

[68] C. Verdi, F. Caruso, and F. Giustino, Nat. Commun. **8**, 1 (2017).

[69] H. Hübener, U. De Giovannini, and A. Rubio, Nano Lett. **18**, 1535 (2018).

[70] D. Sangalli, A. Ferretti, H. Miranda, C. Attaccalite, I. Marri, E. Cannuccia, P. Melo, M. Marsili, F. Paleari, A. Marrazzo *et al.*, J. Phys.: Condens. Matter **31**, 325902 (2019).